Experiments on a Flettner rotor at critical and supercritical Reynolds numbers

Bordogna, G.; Muggiasca, S.; Giappino, S.; Belloli, M.; Keuning, J. A.; Huijsmans, R. H.M.; van 't Veer, A. P.

DOI
10.1016/j.jweia.2019.02.006

Publication date
2019

Document Version
Final published version

Published in
Journal of Wind Engineering and Industrial Aerodynamics

Journal of Wind Engineering & Industrial Aerodynamics 188 (2019) 19–29

Contents lists available at ScienceDirect

Journal of Wind Engineering & Industrial Aerodynamics

journal homepage: www.elsevier.com/locate/jweia

Experiments on a Flettner rotor at critical and supercritical Reynolds numbers

G. Bordogna [a,*], S. Muggiasca [b], S. Giappino [b], M. Belloli [b], J.A. Keuning [a], R.H.M. Huijsmans [a], A.P. van 't Veer [a]

[a] Section of Ship Hydromechanics, Delft University of Technology, Mekelweg 2, 2628, CD, Delft, The Netherlands
[b] Department of Mechanical Engineering, Politecnico di Milano, Via La Masa 1, 20156, Milan, Italy

ARTICLE INFO

Keywords:
Rotor sail
Rotating cylinder
Magnus effect
Wind assisted ship propulsion
Pressure measurements
Wind tunnel tests

ABSTRACT

The Flettner rotor is attracting increasing attention as a viable technology for wind-assisted ship propulsion. Nonetheless, the influence of the Reynolds number on the aerodynamic performance of rotating cylinders is still unclear and under debate. The present study deals with a series of wind-tunnel experiments on a large-scale Flettner rotor in which the forces and pressures acting on the cylinder were measured for Reynolds numbers as large as $Re = 1.0 \cdot 10^6$. The rotating cylinder used in the experimental campaign had a diameter of 1.0 m and span of 3.73 m. The results indicate that the lift coefficient is only affected by the Reynolds number in the critical flow region and below velocity ratio $k = 2.5$. Conversely, in the velocity ratio range $1 < k \leq 2.5$, the drag coefficient is markedly influenced by the Reynolds number over the entire range of flow conditions analyzed. The power coefficient scales with the cube of the tangential velocity and it appears to be insensitive to the Reynolds number or whether the cylinder is spun in an air stream or in still air.

1. Introduction

The Flettner rotor is a rotating cylinder that generates an aerodynamic lift due to the Magnus effect. Invented by German engineer Anton Flettner (1925), it was first used in 1925 on board the *Backau* ship as a form of propulsion. The *Backau* was equipped with two Flettner rotors and it successfully completed its first voyage across the Atlantic in 1926. The same year, following the success of the first rotor ship, the *Barbara* was launched. The vessel had three Flettner rotors and it served as a freighter in the Mediterranean between 1926 and 1929. Despite the proven concept, the rotor ship was fast abandoned since it could not compete with the increasing adoption of diesel engines and with the low oil price of that time. In present years, however, the possibility to use wind energy as an auxiliary form of propulsion for commercial ships has again become of interest due to the volatile fuel prices and to the ever-stringent environmental regulations.

Since its inception the Flettner rotor was seldom used for real-life applications in the maritime field, nonetheless, the physical phenomena associated with rotating cylinders attracted the interest of many scientists over the years. Among the several parameters that were proven to affect the aerodynamic performance of a Flettner rotor (the velocity ratio, the aspect ratio, the use of endplates and the endplate's size), the influence of the Reynolds number is still a matter of debate as it emerges from the studies conducted on this topic until today.

(Reid, 1924) carried out a systematic series of experiments on a rotating cylinder of aspect ratio $AR = 13$, without endplates, at Reynolds numbers varying between $Re = 3.9 \cdot 10^4$ and $Re = 1.1 \cdot 10^5$. The results of (Reid, 1924) indicate that for the range considered, the Reynolds number has a marginal influence on C_L and C_D. The work of Thom represents an important contribution to the research on Flettner rotors. The author, in fact, conducted a large series of force and pressure measurements of rotating cylinders, studying the influence of surface roughness, aspect ratio as well as endplates on the aerodynamic forces. Concerning the topic of scale effects, in (Thom, 1934), the lift and drag coefficients were measured on a rotating cylinder of aspect ratio $AR = 12.5$ at $Re = 5.3 \cdot 10^4$ and $Re = 8.8 \cdot 10^4$. The results indicate that the effects of different Reynolds numbers on the aerodynamic coefficients is negligible.

Several years after (Swanson, 1961), provided a detailed summary of the experiments on rotating cylinders carried out until that time. Results of a set of two-dimensional tests performed by the author in the Reynolds number range $3.5 \cdot 10^4 < Re < 5.0 \cdot 10^5$ for velocity ratios $0 \leq k \leq 1$, were also reported. A remarkable output of this investigation is that, for

* Corresponding author.
E-mail address: g.bordogna@tudelft.nl (G. Bordogna).

https://doi.org/10.1016/j.jweia.2019.02.006
Received 3 September 2018; Received in revised form 1 February 2019; Accepted 17 February 2019
Available online 2 March 2019

Nomenclature

AR	Aspect ratio H/D
$Area_s$	Cylinder surface area, $\pi \cdot D \cdot H$
C_d	Sectional drag coefficient, $F_d/(0.5 \cdot \rho \cdot V^2 \cdot H \cdot D)$
C_D	Overall drag coefficient, $F_D/(0.5 \cdot \rho \cdot V^2 \cdot H \cdot D)$
C_f	Cylinder skin friction coefficient
C_l	Sectional lift coefficient $F_l/(0.5 \cdot \rho \cdot V^2 \cdot H \cdot D)$
C_L	Overall lift coefficient, $F_L/(0.5 \cdot \rho \cdot V^2 \cdot H \cdot D)$
C_p	Pressure coefficient, $Pressure/(0.5 \cdot \rho \cdot V^2)$
C_{pow}	Power coefficient in an air stream, $Power/(0.5 \cdot \rho \cdot V^3 \cdot H \cdot D)$
$C_{pow-NoW}$	Power coefficient in still air, $Power_{NoW}/(0.5 \cdot \rho \cdot V^3 \cdot H \cdot D)$
D	Cylinder diameter
F_l, F_d	Sectional lift and drag force
F_L, F_D	Overall lift and drag force
H	Cylinder span
k	Velocity ratio, U_{tan}/V
$Power$	Power consumption in an air stream
$Power_{NoW}$	Power consumption in still air
Re	Reynolds number, $(V \cdot D)/\nu$
U_{tan}	Cylinder tangential velocity
V	Incoming flow velocity
ν	Kinematic viscosity of air
ρ	Density of air

$0 \leq k \leq 0.5$ and $1.3 \cdot 10^5 < Re < 5.0 \cdot 10^5$, the lift coefficient becomes negative and the drag coefficient appears to be considerably affected by the variation of the Reynolds number up to $k = 0.75$.

During the oil crisis in the 1980s, wind assistance for ship propulsion was considered an appealing manner to cut operational costs and this led to several publications on the topic. Relevant to the present study is the work of (Clayton, 1985) and (Bergeson and Greenwald, 1985). The former author performed experiments at two different Reynolds numbers, namely $Re = 1.7 \cdot 10^4$ and $Re = 4.9 \cdot 10^4$, on a rotating cylinder of aspect ratio $AR = 10.4$ equipped with two endplates of size $1.4D$ and, subsequently, $2D$. The study indicates that when the larger endplate size is adopted the results seem to be insensitive to the different Reynolds numbers considered. Nonetheless, for the smaller endplate size, the author concludes that a lower Reynolds number causes a decrease in C_L and an increase in C_D. This effect is noticed until velocity ratio $k = 2$. Conversely, Bergeson and Greenwald mounted a rotating cylinder with diameter $D = 1.16$ m and $H = 7.2$ m on aboard a small motor yacht. Using a combination of mooring lines and spring dynamometers, the authors could measure the forces generated by the rotor for a variety of velocity ratios. The authors report that the tests were conducted with a wind speed ranging between 9 and 16 knots, meaning that, on average, the Reynolds number achieved was in the order of $Re = 5.0 \cdot 10^5$. The results show that, for velocity ratio $k < 3$, C_L is larger than the lift coefficients obtained in other experiments carried out on rotating cylinders of similar aspect ratios but at lower Reynolds numbers. No results of the drag coefficients are provided.

In 1993 (Tokumaru and Dimotakis, 1993), completed a series of tests on a rotating cylinder of aspect ratio $AR = 18.7$, with no endplates, at $Re = 3.8 \cdot 10^3$. The authors report that, for low velocity ratios, their results overestimate the lift coefficient compared with the data provided by (Reid, 1924), and they attribute the discrepancy to a lower Reynolds number used in their experimental campaign.

More recent are the studies of (Badalamenti, 2010) and (Zhang et al., 2013). The former conducted a series of tests on a cylinder of aspect ratio $AR = 5.1$ with no endplates, at Reynolds numbers ranging between $Re = 1.9 \cdot 10^4$ and $Re = 9.6 \cdot 10^4$. The results partially disagree with those of (Clayton, 1985): a decrease in Reynolds number entails an increase in C_L as well as in C_D. This is particularly noticeable for $k < 1.5$ (C_L) and for $k > 2.5$ (C_L and C_D). For a similar Reynolds number ($Re = 4.0 \cdot 10^4$), the latter author carried out wind-tunnel experiments on a rotating cylinder with $AR = 6$. The data show a similar trend compared to the results of (Badalamenti, 2010).

Besides the experimental studies, several CFD simulations on the topic of rotating cylinders were also published over the years. Among these, research efforts as (Badr et al., 1989), (Ingham and Tang, 1990), (Chew et al., 1995), (Mittal and Kumar, 2003) and (Padrino and Joseph, 2006) dealt with two-dimensional flows at low Reynolds numbers ($Re < 1.0 \cdot 10^3$). In (Badr et al., 1989) is shown that simulations conducted at $Re = 60$ lead to a lower lift coefficient than when $Re = 5$ is used. These results also agree with the findings of (Ingham and Tang, 1990). (Mittal and Kumar, 2003) and (Padrino and Joseph, 2006) conducted simulations at $Re = 200$ and, at $k = 4$, both studies indicate that $C_L \approx 18$ and $C_D \approx 0$. Conversely, in (Chew et al., 1995), whose computations were carried out at $Re = 1.0 \cdot 10^3$, is reported that, at velocity ratio $k = 4$, $C_L \approx 9$ and $C_D \approx 3.5$. Arguably, such significant discrepancy between the results of (Mittal and Kumar, 2003) and those of (Padrino and Joseph, 2006) is, at least partially, due to the different Reynolds numbers used in their computations.

(Karabelas, 2010) carried out Large Eddy Simulations on a cylinder at $Re = 1.4 \cdot 10^5$ up to velocity ratio $k = 2$. The results are compared with experimental data obtained at $Re = 6.0 \cdot 10^4$ and reported in (Aoki and Ito, 2001). The comparison indicates that the drag coefficient is generally unaffected by the Reynolds number, whereas, at $k = 1$, the lift coefficient achieved at $Re = 1.4 \cdot 10^5$ is approximately twice as large that one obtained at $Re = 6.0 \cdot 10^4$. In another study (Karabelas et al., 2012), completed a series of two-dimensional CFD simulations on a rotating cylinder at $Re = 5.0 \cdot 10^5$, $Re = 1.0 \cdot 10^6$ and $Re = 5.0 \cdot 10^6$ for velocity ratio range $2 \leq k \leq 8$. The results suggest that the lift and drag coefficients are only marginally affected by the Reynolds number and that, in general, a higher Reynolds number leads to lower force coefficients. On the other hand (Everts et al., 2014), who conducted a study at the same Reynolds numbers as (Karabelas et al., 2012), concludes that the Reynolds number has a marked influence on C_l and C_d: an increase in Reynolds number produces a sharp increase in lift coefficient and a decrease in drag coefficient.

The works of (Zhang and Bensow, 2011), (Craft et al., 2012), (Li et al., 2012) and (De Marco et al., 2014) deal with rotating cylinders immersed in a three-dimensional flow at relatively high Reynolds numbers (Zhang and Bensow, 2011). show that, for the two Reynolds numbers considered ($Re = 5.0 \cdot 10^4$ and $Re = 1.0 \cdot 10^5$) the lift and drag coefficients are substantially insensitive to scale effects (Craft et al., 2012). carried out a series of computations on a Flettner rotor at three different Reynolds numbers: $Re = 1.4 \cdot 10^5$, $Re = 8.0 \cdot 10^5$ and $Re = 1.0 \cdot 10^6$. The outcome of the investigation is that the effect of the Reynolds number on the lift coefficient is marginal, both for the bare cylinder and when endplates are used. No results for the drag coefficient are reported (Li et al., 2012). performed simulations on a series of Flettner rotors with aspect ratios 3, 6, 9 and 12 at $Re = 1.6 \cdot 10^6$. Comparing the results for the case with $AR = 6$ and the experimental data of (Badalamenti, 2010), in which $AR = 5.1$ and $Re = 9.6 \cdot 10^4$, it appears that, for velocity ratios $k < 3$, the higher Reynolds number leads to higher lift coefficients. Conversely, the drag coefficient seems unaffected by the change in flow regime. Finally, the study of (De Marco et al., 2014) deals with CFD simulations at $Re = 5.11 \cdot 10^6$ of a Flettner rotor of aspect ratio $AR = 3.5$, with and without endplates. For the case with endplates (size $= 2D$), and for $1 < k < 3$, it is

shown that both C_L and C_D are larger than the results reported by (Reid, 1924), (Thom, 1934), (Badalamenti, 2010) and (Zhang and Bensow, 2011). It should be noticed, however, that a direct comparison of these results is hindered by the use of different aspect ratios.

From an operational perspective, another important aspect of Flettner rotors is the power necessary to spin the cylinder at the desired rotational velocity. In (Reid, 1924) is reported that the power consumption of the rotating cylinder was greater in still air than in an air stream (Zhang and Bensow, 2011). also indicate that, for a given cylinder, the freestream velocity influences the power requirement, being lower for a higher freestream velocity. The results of (Clayton, 1985) and (Badalamenti, 2010) disagree with these findings as their data show that the power necessary to spin the cylinder is insensitive to the Reynolds number.

For the interested reader, other studies on rotating cylinders not included in this summary can be found in (Zdravkovich, 2003).

The review here presented indicates that, despite the numerous publications, the influence of the Reynolds number on the aerodynamic coefficients of a rotating cylinder is still unclear. This is due to two main reasons. The first reason is that most of the available experimental data were obtained at Reynolds numbers in the subcritical regime or lower. Only (Swanson, 1961) carried out experiments at higher Reynolds numbers but, in this case, the velocity ratio was limited to $k = 1$. On the other hand, the computational investigations that did extend to the supercritical regime show contradictory results. Arguably, engineering challenges as for instance having the possibility to make use of an adequate facility both in terms of dimensions and maximum reachable flow speed, as well as having to deal with large aerodynamic forces and moments, hindered the executions of experiments in the supercritical regime. Different complexities, but certainly not less troublesome, are those related to the CFD simulations of a rotating cylinder at high Reynolds numbers. In this respect, the results of (Zhang and Bensow, 2011) are exemplary: for a same condition, the lift and drag coefficients show a considerable scatter depending on the type of flow solver employed for the computations.

In this context, the present work deals with a series of wind-tunnel experiments aimed at the understanding of the Reynolds number effect on the aerodynamic coefficients of a rotating cylinder in a critical and supercritical flow regime. The tests were carried out on a large-scale Flettner rotor (referred to as Delft Rotor in the text) and the aerodynamic forces, as well as the pressures on the cylinder's surface, were measured at all tested conditions. A set of different Reynolds numbers was investigated, being, respectively, $Re = 1.8 \cdot 10^5$ the lowest and $Re = 1.0 \cdot 10^6$ the highest Reynolds numbers achieved.

2. Experimental setup

2.1. The Delft Rotor

The experiments were carried out in the boundary-layer test section of Politecnico di Milano wind tunnel. The test section is 13.84 m wide, 3.84 m high and 35 m long. During the experimental campaign, the Delft Rotor was mounted in the centre of the test chamber as shown in Fig. 1.

The Delft Rotor is a rotating cylinder with diameter $D = 1.0$ m and span $H = 3.73$ m and it is comprised of three main parts: a fixed structure, an internal frame and an outer skin. The fixed structure consisted of a lower and an upper assembly made of four threaded bars screwed into the wind-tunnel ground and ceiling structural beams. Two purpose-built force balances were placed at the extremity of the threaded bars, on top of which the bearing housings were bolted. The proximity of the balances to the bearings minimized the bending moment and allowed to use a three-component force balance built to measure lift, drag and torque. The outer skin was composed of four calendered aluminium sheets bolted to the internal frame. The frame, composed of three equal wheels and a set of vertical bars, was rotated by an electric engine hung to the lower bearing housing (Fig. 2). The Delft Rotor was equipped with two different

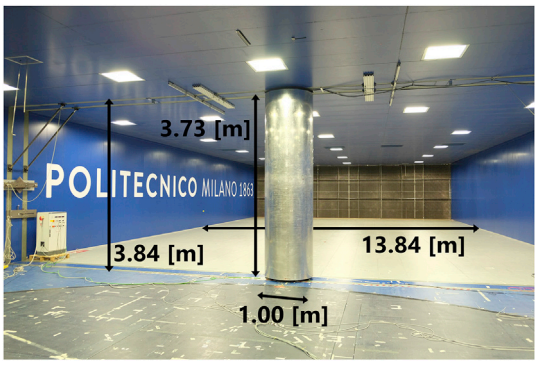

Fig. 1. The Delft Rotor in Politecnico di Milano wind tunnel.

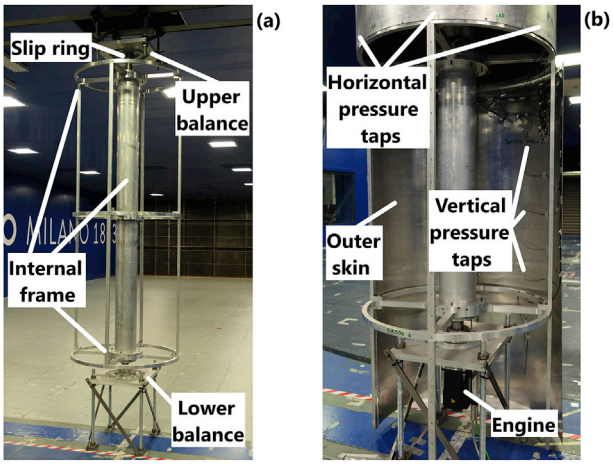

Fig. 2. Structure of the Delft Rotor without (a) and with (b) outer skin.

pressure measurement systems, namely one high sample-rate pressure scanner (PSI ESP-32HD) and one AMS 4711 sensor. The reason to use two different measurement systems is that limited literature was found on techniques for dynamic pressure measurements. Therefore, it was decided to use two measurement systems with different characteristics. The ESP scanner, that has a pressure range of ±2500 Pa, has 32 channels, and this allows to take several pressure measurements simultaneously. Due to its dimensions, it had to be fixed to the central shaft of the internal frame of the cylinder, meaning that, during the tests, it was only marginally affected by the centripetal acceleration but also that, to reach all the pressure taps, long pneumatic connections had to be made. Conversely, the AMS system, that has a pressure range of ±2000 Pa, is a very compact instrument with only one pressure tap and thus could be directly placed on the internal face of the cylinder outer skin. This means that the AMS system was more affected by the centripetal acceleration, but it had a very short pneumatic connection. Although in a different manner, both the centripetal acceleration and the pneumatic connection influence the pressure measurements, and, in general, such influence increases with the rotational speed. Corrections were made to compensate for these effects as far as possible, nonetheless, the errors that could have derived from such effects are taken into account in the measurement uncertainty analysis reported in Section 2.3. Further information on the experimental setup and on the pressure correction methods employed can be found in (Bordogna et al., 2018).

The experimental campaign on the Delft Rotor comprised two distinct series of tests. During the first series of tests, all the 32 ESP scanner pressure taps were equally distributed around the cylinder circumference at 1.85 m from the ground (horizontal pressure taps). Doing so, it was possible to measure the pressure distribution around an entire section at the cylinder mid-height during the tests carried out at $k = 0$ (static

experiments).

During the second series of tests, 16 taps were removed from the circumference and they were equally spaced along the span of the cylinder (vertical pressure taps). This second type of arrangement was used to measure the pressure distribution on the Delft Rotor at different heights. Similarly to the ESP system, also the AMS 4711 sensor was placed at 1.85 m from the ground (cylinder mid-height). The pressure systems installed on the Delft Rotor use a piezoresistive silicon chip as sensing element and they both work as differential transducers. Thus, to obtain the actual pressure acting on the outer skin, it was necessary to measure also the static pressure in the interior of the cylinder. This was achieved using a single pressure tube located above the lower force balance. To pass the signal of both the ESP scanner and the AMS 4711 sensor to the readout instrumentation, a slip ring connected to the upper hollow shaft was installed (Fig. 2). The slip ring was also equipped with a transducer to measure the instantaneous velocity and angular position. The angular position of the cylinder was therefore in phase with the pressure measurements.

Table 1
Overall lift and drag coefficients - measurement uncertainties with 95% confidence level.

Coeff.	*Re*	Velocity ratio *k*										
	[$\cdot 10^5$]	0	0.5	1.0	1.5	2.0	2.5	3.0	3.5	4.0	4.5	5.0
C_L	1.8	0.212	0.266	0.241	0.235	0.321	0.262	–	–	–	–	–
	2.5	0.135	0.184	0.234	0.224	0.204	0.182	0.142	0.153	0.119	0.117	0.128
	3.6	0.068	0.089	0.084	0.112	0.098	0.166	0.102	0.098	0.087	0.086	0.132
	10.0	0.081	0.065	0.157	0.115	0.049	–	–	–	–	–	–
C_D	1.8	0.213	0.259	0.221	0.216	0.269	0.328	–	–	–	–	–
	2.5	0.113	0.477	0.374	0.233	0.210	0.114	0.112	0.124	0.308	0.421	0.556
	3.6	0.072	0.161	0.068	0.085	0.062	0.111	0.181	0.218	0.275	0.384	0.523
	10.0	0.050	0.007	0.080	0.055	0.098	–	–	–	–	–	–

Table 2
Sectional lift and drag coefficients - measurement uncertainties with 95% confidence level.

Coeff.	*Re*	Velocity ratio *k*										
	[$\cdot 10^5$]	0	0.5	1.0	1.5	2.0	2.5	3.0	3.5	4.0	4.5	5.0
C_l	1.8	0.241	0.139	0.115	0.198	0.237	0.157	–	–	–	–	–
	2.5	0.154	0.105	0.101	0.112	0.105	0.172	0.363	0.456	0.440	0.395	0.419
	3.6	0.140	0.051	0.143	0.191	0.142	0.142	0.356	0.469	0.474	0.446	0.435
	10.0	0.125	0.078	0.356	0.025	0.223	–	–	–	–	–	–
C_d	1.8	0.197	0.104	0.128	0.112	0.159	0.146	–	–	–	–	–
	2.5	0.105	0.101	0.120	0.111	0.100	0.108	0.104	0.143	0.164	0.101	0.148
	3.6	0.054	0.048	0.082	0.067	0.079	0.059	0.047	0.099	0.119	0.052	0.148
	10.0	0.097	0.011	0.084	0.111	0.144	–	–	–	–	–	–

Table 3
Sectional pressure coefficients - measurement uncertainties with 95% confidence level.

Coeff.	*Re*	Velocity ratio *k*										
	[$\cdot 10^5$]	0	0.5	1.0	1.5	2.0	2.5	3.0	3.5	4.0	4.5	5.0
C_{pmin}	1.8	0.445	0.754	0.767	0.732	0.737	0.737	–	–	–	–	–
	2.5	0.149	0.396	0.374	0.379	0.380	0.396	0.547	0.496	0.437	0.457	0.411
	3.6	0.153	0.189	0.177	0.179	0.247	0.306	0.374	0.398	0.364	0.309	0.329
	10.0	0.121	0.105	0.101	0.075	0.038	–	–	–	–	–	–
C_{pmax}	1.8	0.224	0.730	0.732	0.735	0.755	0.730	–	–	–	–	–
	2.5	0.153	0.375	0.390	0.375	0.375	0.375	0.376	0.375	0.390	0.376	0.383
	3.6	0.092	0.178	0.178	0.176	0.199	0.176	0.179	0.193	0.189	0.176	0.179
	10.0	0.036	0.033	0.059	0.063	0.025	–	–	–	–	–	–

Table 4
Power coefficients - measurement uncertainties with 95% confidence level.

Coeff.	*Re*	Velocity ratio *k*										
	[$\cdot 10^5$]	0	0.5	1.0	1.5	2.0	2.5	3.0	3.5	4.0	4.5	5.0
C_{pow}	1.8	–	0.039	0.077	0.113	0.149	0.185	–	–	–	–	–
	2.5	–	0.020	0.038	0.056	0.115	0.130	0.216	0.343	0.403	0.601	0.905
	3.6	–	0.009	0.018	0.033	0.077	0.095	0.177	0.299	0.401	0.567	0.786
	10.0	–	0.006	0.011	0.027	0.051	–	–	–	–	–	–
$C_{pow-NoW}$	1.8	–	0.039	0.076	0.111	0.147	0.052	–	–	–	–	–
	2.5	–	0.020	0.039	0.058	0.099	0.112	0.182	0.284	0.334	0.571	0.953
	3.6	–	0.010	0.017	0.030	0.061	0.079	0.138	0.262	0.349	0.519	0.714
	10.0	–	0.002	0.006	0.015	0.035	–	–	–	–	–	–

Table 5
Summary of the experiments carried out on the Delft Rotor.

# Experiment	Re	Velocity ratio k x = executed - = not executed													
	[·10⁵]	0	0.5	1.0	1.25	1.5	1.75	2.0	2.25	2.5	3.0	3.5	4.0	4.5	5.0
Exp. 1	1.8	x	–	x	x	x	x	x	x	x	–	–	–	–	–
Exp. 1	3.6	x	–	x	x	x	x	x	x	x	–	–	–	–	–
Exp. 1	5.5	x	–	x	x	x	x	x	x	x	–	–	–	–	–
Exp. 1	10.0	x	–	x	x	x	x	x	–	–	–	–	–	–	–
Exp. 2	1.8	x	x	x	–	x	–	x	–	x	–	–	–	–	–
Exp. 2	2.5	x	x	x	x	x	x	x	x	x	x	x	x	x	x
Exp. 2	3.6	x	x	x	x	x	x	x	x	x	x	x	x	x	x
Exp. 2	10.0	x	x	x	–	x	–	x	–	–	–	–	–	–	–

The experimental setup of the Delft Rotor was designed to find a good compromise between the possibility to achieve as high as possible Reynolds numbers and the structural constraints related to the large aerodynamic forces involved.

2.2. Flow characteristics

The boundary layer test section of Politecnico di Milano wind tunnel has a standard turbulent intensity $I_u = 2\%$ while the boundary layer thickness is about 0.2 m. Considering this turbulent intensity level, the critical Reynolds number region for a circular cylinder is anticipated with respect to smooth flow conditions. The lowest Reynolds number tested, $Re = 1.8 \cdot 10^5$, is in fact already experiencing the drag coefficient reduction typical of the critical flow region.

The flow velocity, used to calculate all the aerodynamic coefficients, was measured with a pitot tube placed 5 m in front of the Delft Rotor at the height of 1.85 m from the ground. The clearance between the cylinder and the wind-tunnel floor and ceiling was 55 mm (Fig. 1). These gaps were necessary to let enough room (considering also a safety margin) for the instrumentation cables. Considering the flow velocity reduction due to the boundary layer and that a gap of 55 mm corresponds to about 1.5% of the cylinder span, it can be assumed that the tip vortices were (at least largely) suppressed by the wind-tunnel upper and lower walls. In this respect, the experiments were conducted in a two-dimensional flow condition. However, the wind-tunnel boundary layer caused the flow to have non-two-dimensional features. In fact, the boundary layer, besides the decrease of the incoming flow velocity near the walls, it also caused a change in pressure distribution around the cylinder ends. On the other hand, outside of the boundary layer, the flow presented a straight profile and no effects caused by the wind-tunnel walls were measured.

The effects of such testing conditions are noticeable by comparing the results of the force coefficients obtained using the pressure distribution measured at the cylinder mid-height (sectional C_l and C_d), and the coefficients obtained from the force balances and the pressure integration along the entire span of the Delft Rotor (overall C_L and C_D). In fact, it can be noticed that, due to the wind-tunnel boundary layer, the sectional lift and drag coefficients are, in general, larger than the corresponding overall coefficients.

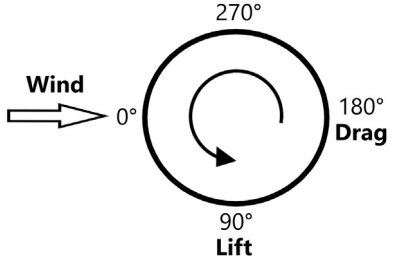

Fig. 3. Cylinder direction of rotation and conventions used.

2.3. Measurement uncertainty

The experimental uncertainty was calculated according to the ISO "Guide to the Expression of Uncertainty in Measurement" (ISO/IEC 98-3, 2008). The expanded uncertainty with 95% confidence level, u_{95}, was calculated from the standard uncertainty related to the measurement precision, u_{pr}, and the standard uncertainty of the bias errors of the measurement instruments, u_{bias}. For each quantity of interest, u_{pr} was obtained using the data of repeated experiments as well as data of one same experiment but measured with different instruments. These are the force balances and the ESP pressure scanner for the overall C_L and C_D, the ESP pressure scanner and the AMS 4711 sensor for the sectional C_l, C_d and C_p, and the force balances and the engine controller for C_{pow}. The standard uncertainty related to the measurement precision reads:

$$u_{pr} = \sqrt{(\sigma^2/N)} \tag{1}$$

where σ is the standard deviation of the N considered data points. Conversely, the standard uncertainty related to the bias errors of the measurement instrument is the sensitivity of the measurement instrument accuracy (as per specification of the manufacturer or, in case of the in-house built force balances, it was measured during the calibration tests) respect to the quantity of interest. u_{bias} can then be calculated by taking the partial derivative of the instrument accuracy with respect to the quantity to be analyzed. The expanded uncertainty with 95% confidence level is thus calculated according to:

$$u_{95} = c \cdot \sqrt{\left(u_{pr}^2 + u_{bias}^2\right)} \tag{2}$$

where the coverage factor c is set to $c = 2$. The measurement uncertainties with 95% confidence level reported in Table 1 (overall C_L and C_D), Table 2 (sectional C_l and C_d), Table 3 (C_{pmin} and C_{pmax}), and Table 4 (C_{pow} and $C_{pow-NoW}$), should be referred to the mean value of all data reported for a given case.

It was not possible to calculate the uncertainty relative to the measurements carried out at $Re = 5.5 \cdot 10^5$ since for each velocity ratio there was only a single data point. Also, for this Reynolds number, it was not possible to measure the pressure inside the rotating cylinder due to a technical issue, meaning that the pressure coefficient curves are unavailable for this test.

3. Results

The results of the experimental campaign on the Delft Rotor are presented in this section. For each velocity ratio, it is reported every measurement carried out, apart from $k = 0$ for which just the averaged result is shown for the sake of clarity. It should be noticed that the results of the static measurements ($k = 0$) given in Fig. 4 – Fig. 9 use the same colour legend as used for all other cases to indicate the corresponding Reynolds number. All measurement techniques employed in the experiments are indicated in the result figures: force balances (F. Balance), integration of the results of ESP scanner vertical pressure sensors (Press.

Int.), AMS 4711 pressure sensor (AMS47), ESP scanner horizontal pressure sensors (Scanner) and, finally, (Engine) for the engine controller used to measure the power consumption. As stated in Section 2.1, two separate series of tests were carried out on the Delft Rotor. This is specified in the result figures with the terminology "Exp. 1" (first test series) and "Exp. 2" (second test series). Regarding the integration of the pressure results of the vertical ESP scanner sensors, the pressures measured by the 16 taps installed along the cylinder span were used in

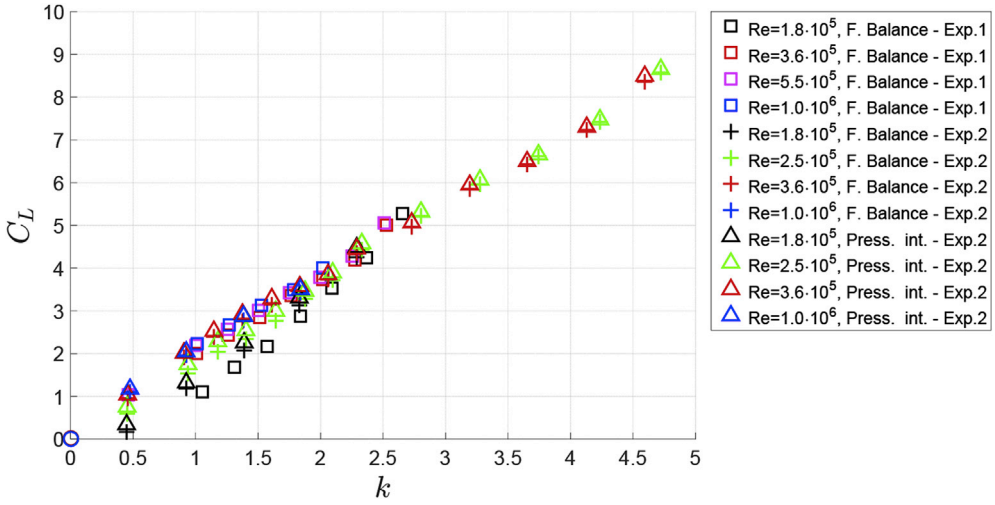

Fig. 4. Overall lift coefficient vs velocity ratio.

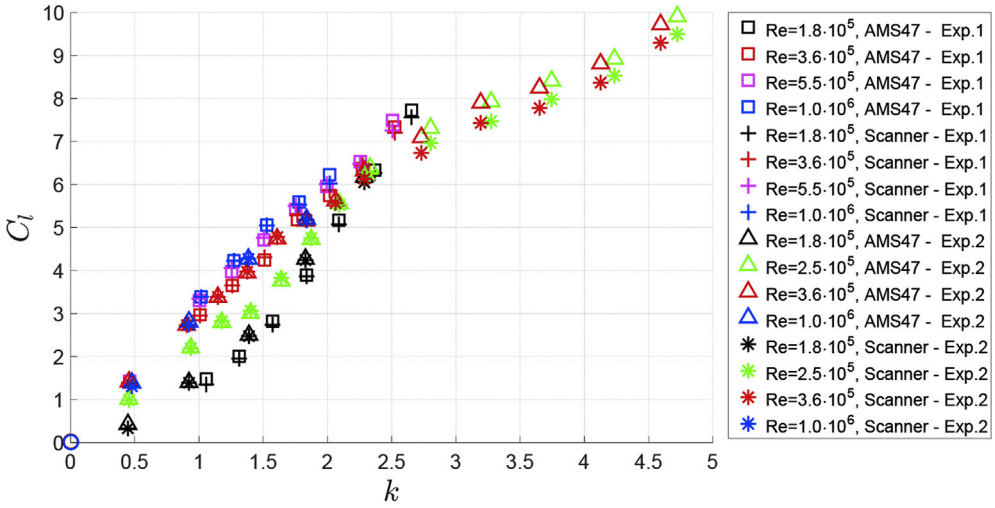

Fig. 5. Sectional lift coefficient vs velocity ratio.

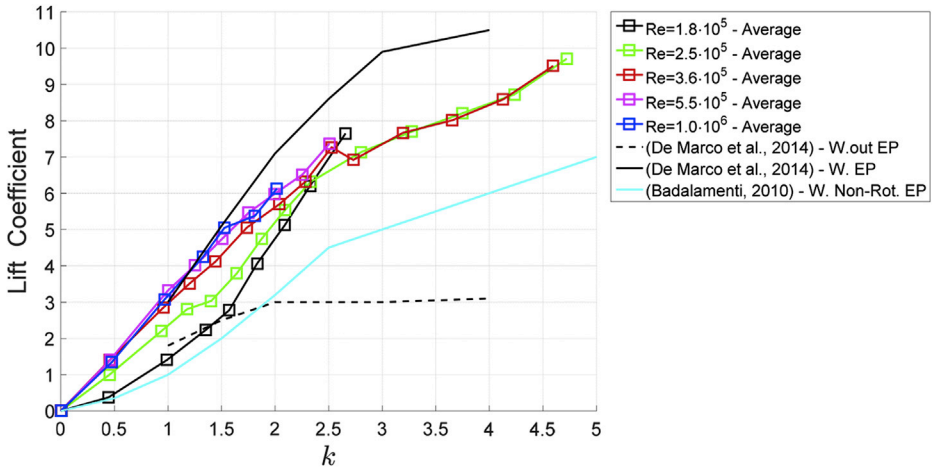

Fig. 6. Comparison of averaged sectional lift coefficient with other similar studies.

the calculations. The integrated pressure was then transformed into non-dimensional coefficients by using the reference wind speed measured by the pitot tube placed at a height of 1.85 m from the ground (see Section 2.2).

A summary of the cases investigated is given in Table 5.

To better understand the results reported in the following sections, the cylinder direction of rotation and the conventions used in the present analysis are depicted in Fig. 3.

3.1. Lift coefficient

The overall and sectional lift coefficients (Figs. 4 and 5) show a similar trend, as C_L and C_l appear to be affected by the Reynolds number in a similar manner. In the range $0 < k < 2.5$, higher Reynolds numbers

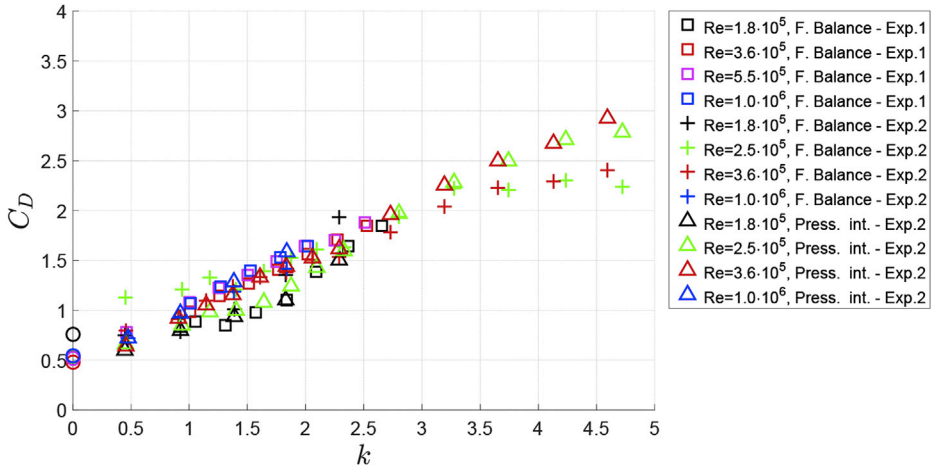

Fig. 7. Overall drag coefficient vs velocity ratio.

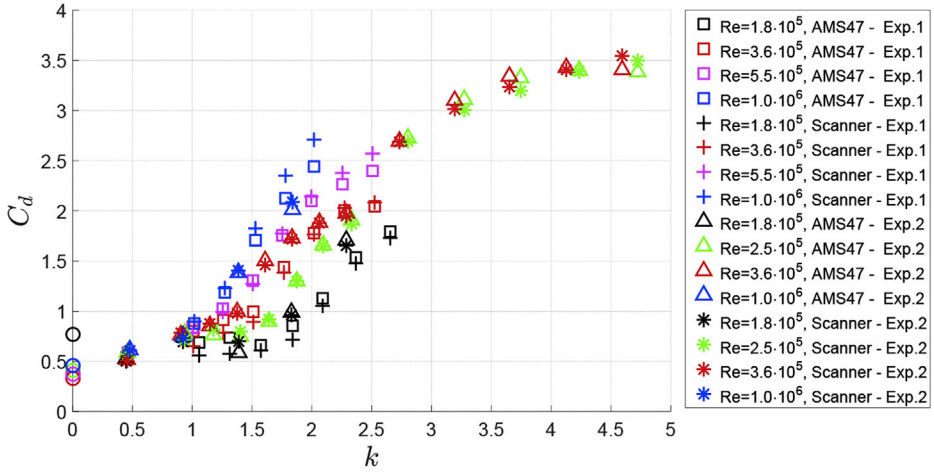

Fig. 8. Sectional drag coefficient vs velocity ratio.

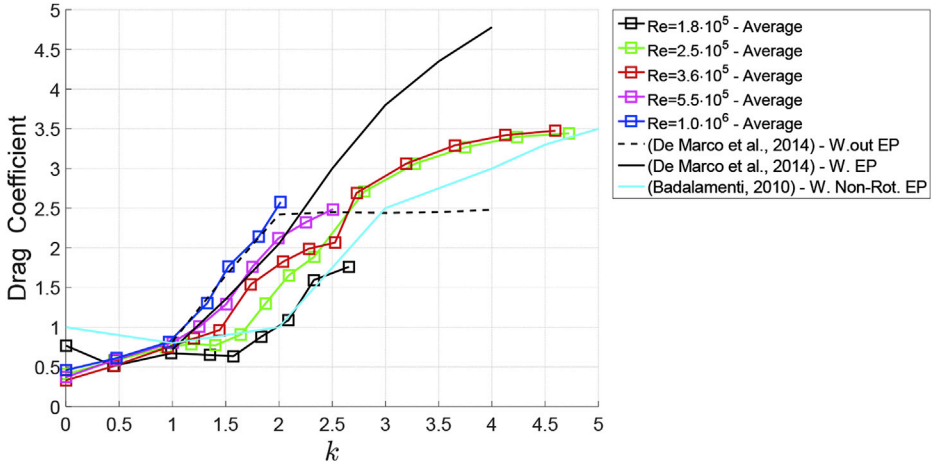

Fig. 9. Comparison of averaged sectional drag coefficient with other similar studies.

lead to higher lift coefficients. This holds true until $Re = 2.5 \cdot 10^5$, in fact for the higher Reynolds numbers considered such difference is no longer appreciable. On the other hand, for velocity ratios $k > 2.5$, the lift coefficient does not seem affected by the Reynolds number. This is also supported by the fact that the influence of the Reynolds number on the lift coefficient appears to decrease with the increase of the velocity ratio.

Studies on three-dimensional cylinders without endplates, as for example (Badalamenti, 2010), and (Li et al., 2012) and (De Marco et al., 2016) indicate that the lift coefficient ceases to increase after a certain velocity ratio and that this depends on the aspect ratio of the cylinder. In (De Marco et al., 2014) simulations on a cylinder with an aspect ratio similar to the present study ($AR = 3.5$) are carried out at $Re = 5.11 \cdot 10^6$. The results show that, for the case without endplates, the lift coefficient reaches a plateau at $k = 2$ (Fig. 6). In the present results, for the range of velocity ratios considered, such plateau is not found, and this is because the tip vortices that generate on a free-standing cylinder are in the current case largely suppressed by the wind-tunnel walls. In fact, as shown in (Li et al., 2012) and (Zhang et al., 2013) the tip vortices dissipate circulation and thus reduce the lift generated by the rotating cylinder. On the other hand, for the same aspect ratio $AR = 3.5$, the lift coefficient results of the cylinder with endplates reported in (De Marco et al., 2014) are more comparable with the results of the present study, especially for $k < 1.5$. Although for a larger aspect ratio ($AR = 5.1$), the results of (Badalamenti, 2010) regarding a Flettner rotor with two non-rotating endplates of size $2D$ show a similar trend compared to the results of the lift coefficients obtained in the present study (Fig. 6). In fact, also in (Badalamenti, 2010) the slope of the lift coefficient curve decreases at $k = 2.5$ and until $k = 5.0$ no plateau is found. On the other hand, compared to the present work, the lift coefficients measured in (Badalamenti, 2010) are considerably lower. It is tenable that this is due to the substantially lower Reynolds number used in the experiments ($Re = 1.9 \cdot 10^4$).

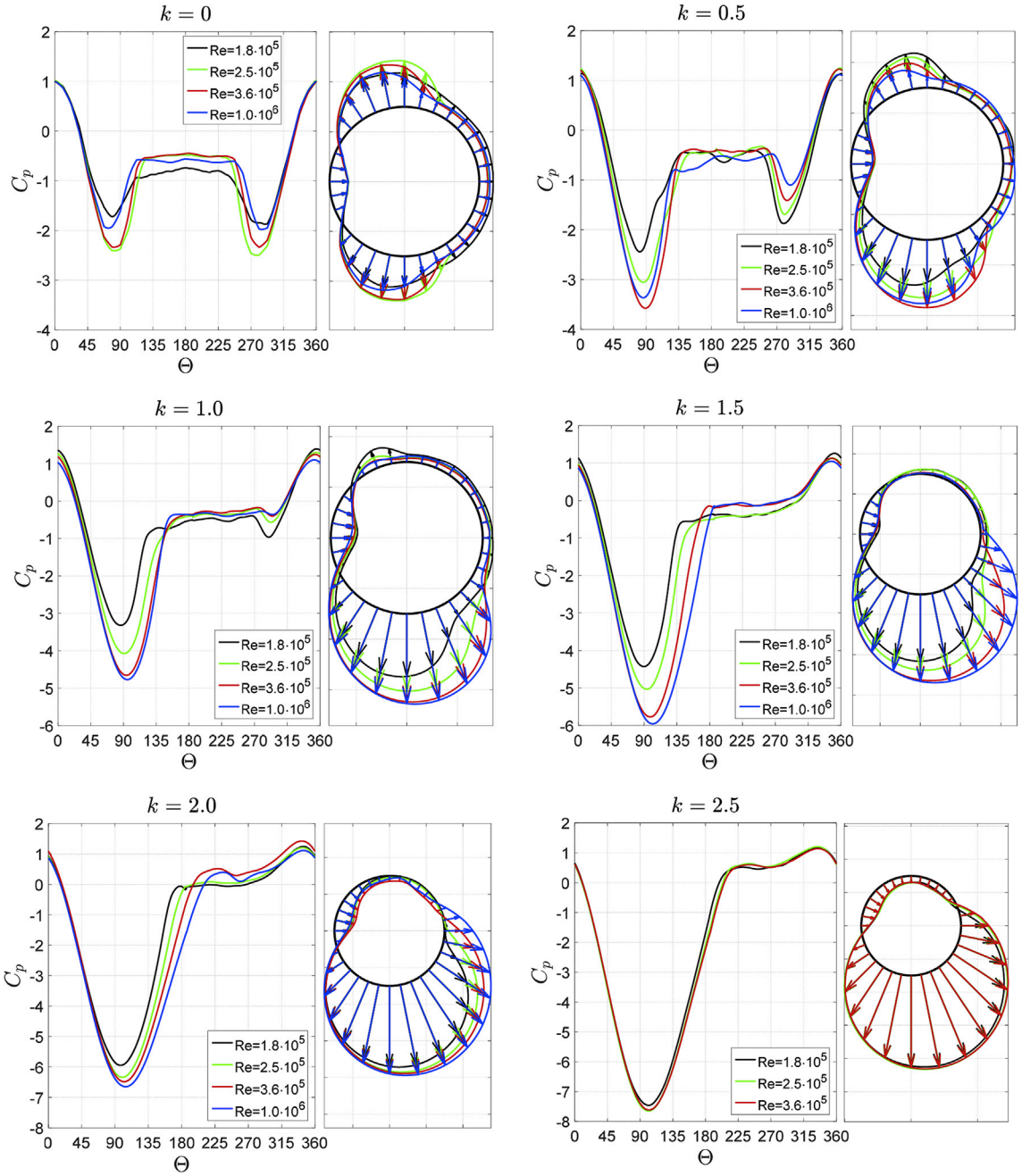

Fig. 10. Averaged sectional pressure coefficients obtained at mid-cylinder span for increasing velocity ratio.k

3.2. Drag coefficient

The large scatter in the overall drag results (Fig. 7) is arguably due to the effect of the wind-tunnel boundary layer on the pressure distributions at the cylinder extremities mentioned in Section 2.2. This scatter is not found in the overall lift coefficient results and this is because the drag coefficient is more sensitive to changes in pressure distribution. In fact, looking at Fig. 10, it can be noticed that a minor shift of the suction peak (that occurs at about 90° with respect to the wind direction) towards the front or the rear of the cylinder would cause a noticeable change in drag force but a marginal change in lift force. The effect of the Reynolds number on the drag coefficient is thus more appreciable in Fig. 8, where the sectional results are reported.

The Reynolds number influence that is evident at $k = 0$ (static cylinder) is suppressed by the rotation at velocity ratio $k = 0.5$. At higher velocity ratios, until $k = 2.5$, the Reynolds number shows a marked influence on the drag coefficient: similar to the lift coefficient, a higher Re entails a higher drag coefficient. Nonetheless, differently from the lift coefficient, the Reynolds number effect is noticed throughout the entire range of Re considered. At $k > 2.5$, the sectional drag coefficients obtained for $Re = 2.5 \cdot 10^5$ and $Re = 3.6 \cdot 10^5$ do not show any remarkable difference. At $k = 2.5$, however, the difference between the drag coefficient obtained at $Re = 1.8 \cdot 10^5$ and $Re = 5.5 \cdot 10^5$ is still substantial.

The findings of (De Marco et al., 2014) show that, in case the cylinder does not have endplates, similarly to the lift coefficient, the drag coefficient ceases to increase at $k = 2$ (Fig. 9). On the contrary, in case the cylinder is equipped with endplates, the drag coefficient keeps increasing with the increase of the velocity ratio. This is also supported by the fact that, according to (Badalamenti, 2010) and (Zhang et al., 2013), for velocity ratios $k > 3$, rotating endplates generate more drag than otherwise a cylinder without or with non-rotating endplates. The results of (Badalamenti, 2010) for the cylinder with two non-rotating endplates

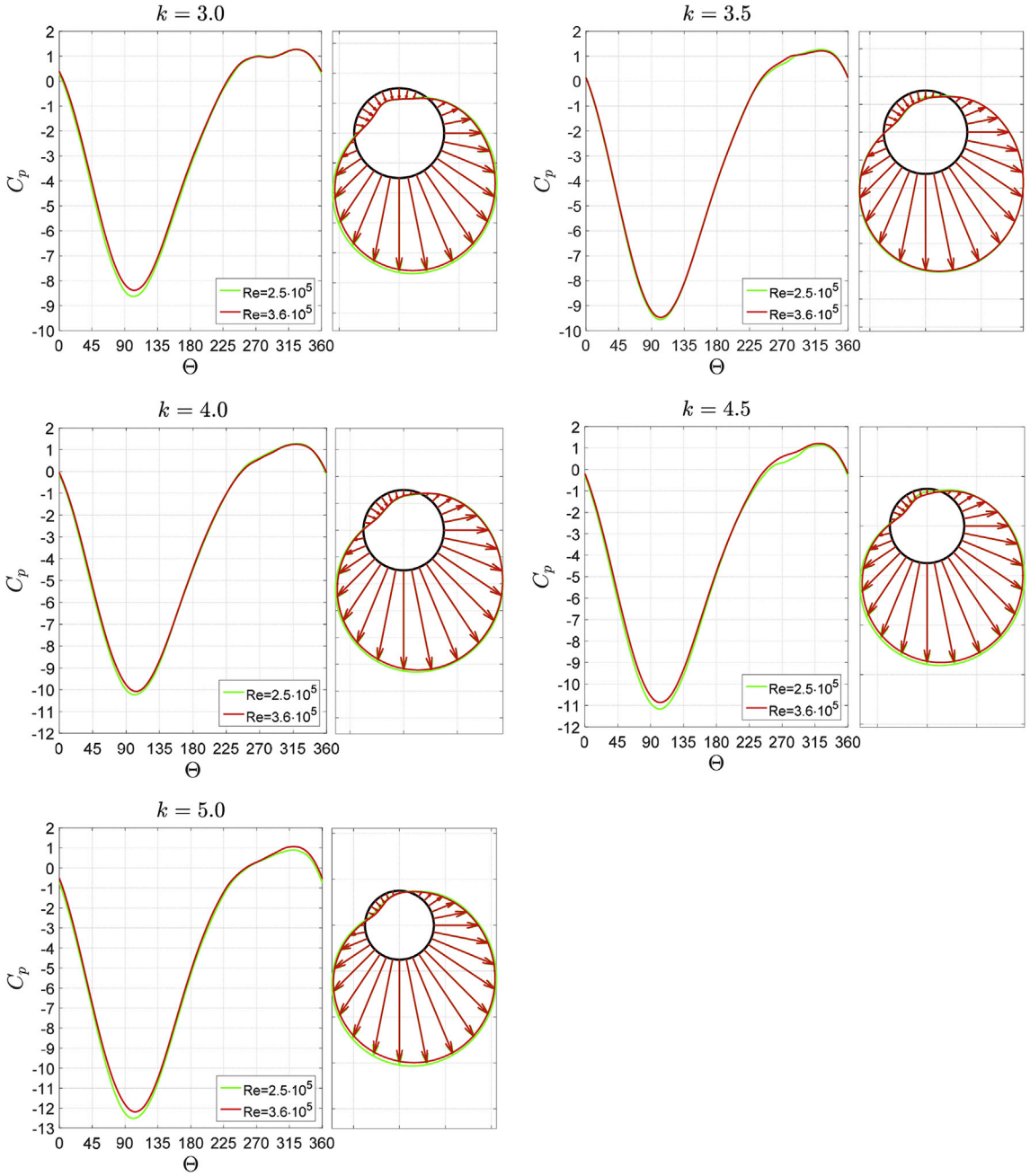

Fig. 10. (*continued*).

show that the slope of the drag coefficient curve decreases at $k = 3$ but no plateau is found up to $k = 5$ (Fig. 9). The results of the present investigation show a similar trend compared to the with the findings of (Badalamenti, 2010) for the case of a cylinder with non-rotating end-plates. Similarly to the lift coefficient, the differences in drag coefficients of the present study and (Badalamenti, 2010), arguably, are at least in part due to the different Reynolds numbers employed.

3.3. Pressure coefficient

The results of sectional pressure coefficient C_p, obtained by averaging the data of the AMS4711 sensor and those of the horizontal pressure taps

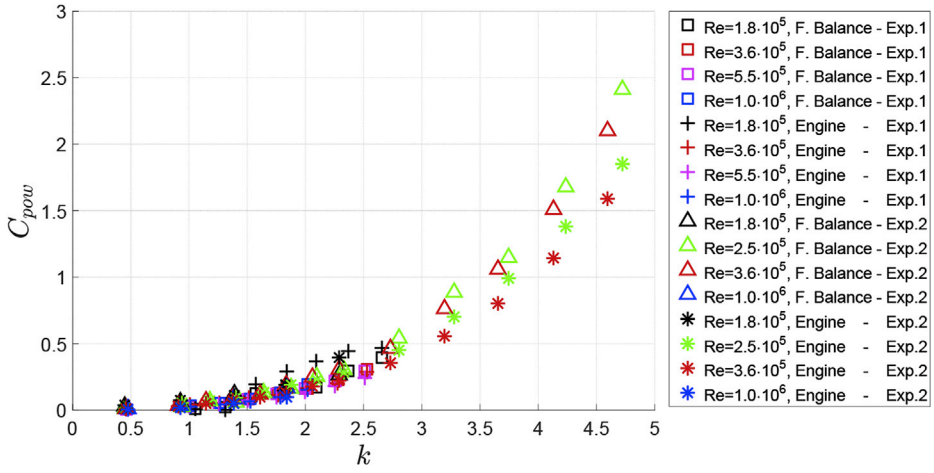

Fig. 11. Power coefficient in an air stream.

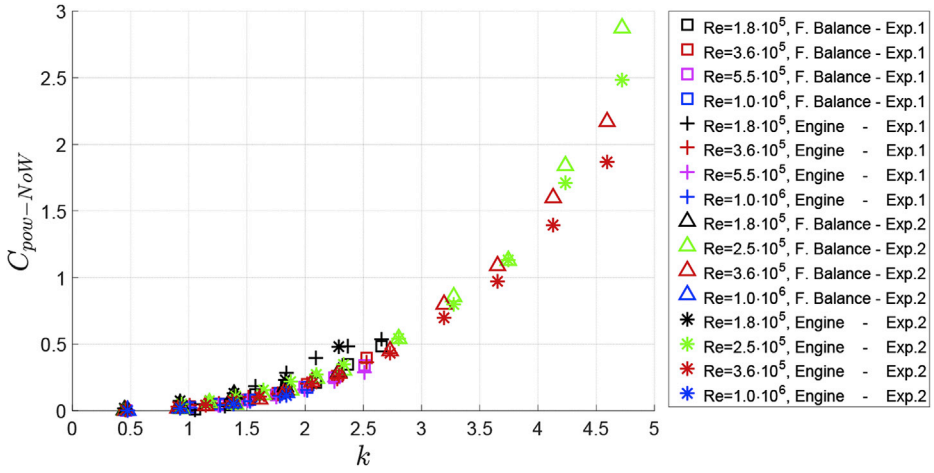

Fig. 12. Power coefficient in still air.

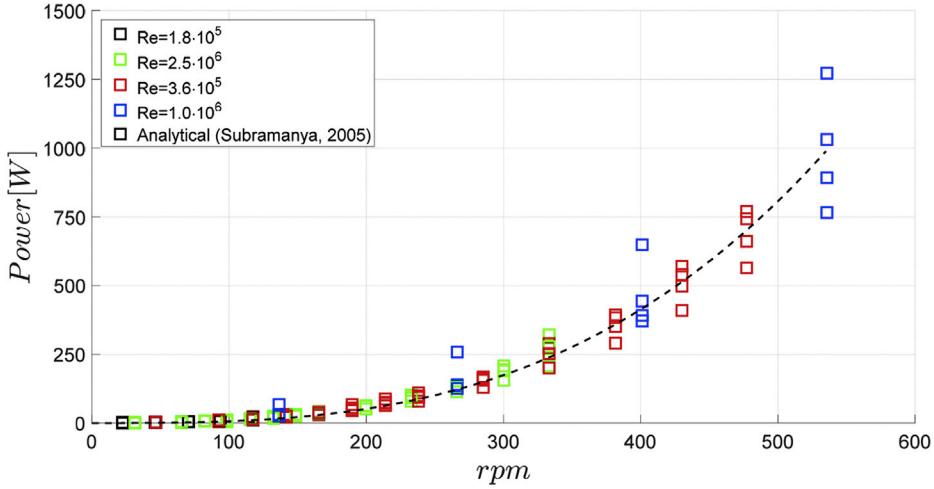

Fig. 13. Delft Rotor power consumption at different rotational speeds.

of the ESP scanner, support the findings of the lift and drag coefficients discussed in Section 3.1 and 3.2.

The cylinder rotation causes an asymmetry in the pressure distribution on the sides of the Flettner rotor that results in the generation of lift (Fig. 10, $k = 0$ and $k = 0.5$).

In the range $0.5 \leq k \leq 2$, a higher Reynolds number leads to a larger C_{pmin} and to a lower C_{pmax}. For $Re = 3.6 \cdot 10^5$ and $Re = 1.0 \cdot 10^6$, this change is balanced in such a way that it results in similar lift coefficients, whereas for the lower Reynolds numbers the change in C_{pmin} and C_{pmax} leads to different lift coefficients as reported in Section 3.1. On the other hand, in the velocity ratio range $1 < k \leq 2.5$, the increase in drag at higher Reynolds numbers is caused by the shift of the suction peak and the separation point towards the rear of the cylinder. On the other hand, for velocity ratios $k > 2.5$, the C_p curves of the two Reynolds numbers tested practically overlap, leading to similar lift and drag coefficients (Figs. 5 and 8). To be noticed is also the shift of the stagnation point with the increase of the velocity ratio in the direction opposite to the direction of rotation of the cylinder (Figs. 3 and 10).

3.4. Power coefficient

The power necessary to spin the cylinder at a given speed was measured during experiments in an air stream as well as in still air. For the sake of comparison, in the case of the tests in still air, the power coefficient was calculated using the wind speed of the corresponding test in an air stream. The results reported in Fig. 11 and Fig. 12 show that the Reynolds number does not influence the power consumption of the Flettner rotor. Also, considering the measurement uncertainties, it can be concluded that the power necessary to spin the cylinder is similar in an air stream and in still air. These findings agree with the results of (Clayton, 1985) and (Badalamenti, 2010).

Fig. 13 indicates that the power consumption scales with the cube of the cylinder tangential velocity. Using the analytical formula proposed by (Subramanya, 2005):

$$Power = C_f \cdot \rho \cdot U_{\tan}^3 / 2 \cdot Area_s \quad (3)$$

A close agreement with the experimental results is found by setting $C_f = 0.007$, that can be considered a reasonable value for the friction coefficient. It should be noticed, however, that the actual power consumption of a Flettner rotor is arguably also affected by the functioning of its mechanical systems.

4. Conclusions

The present study deals with a series of wind-tunnel experiments aimed at a better understanding of the Reynolds number effects on the aerodynamic performance of Flettner rotors. The results indicate that, within the range considered, there is a remarkable influence of the Reynolds number on the lift and drag coefficients below velocity ratio $k = 2.5$. The lift coefficient, in fact, appears to be affected for the two lowest Reynolds numbers tested (critical flow region), but it is insensitive to the Reynolds number in the supercritical flow region ($Re = 3.6 \cdot 10^5$, $Re = 5.5 \cdot 10^5$ and $Re = 1.0 \cdot 10^6$). Also, it appears that the effect of the Reynolds number on the lift coefficient decreases with the increase of the velocity ratio. On the other hand, the drag coefficient is affected by the Reynolds number for all flow conditions analyzed. For velocity ratios until $k = 2.5$, a higher Reynolds number leads to a higher lift and drag coefficient. Conversely, for velocity ratios $k > 2.5$, the results suggest that the effect of the Reynolds number on the lift coefficient becomes limited. Considering that the drag coefficient at $k = 2.5$ appears to be strongly influenced by the different Reynolds numbers tested, the current data arguably do not permit to conclude whether the Reynolds number affects the drag coefficient also for velocity ratios $k > 2.5$.

The results of the present investigation were also compared with similar studies. Despite the discrepancies caused by the substantially different Reynolds numbers used, a qualitative agreement is found with the findings of (Badalamenti, 2010) for the case of a Flettner rotor with two non-rotating endplates.

The power consumption is found to scale with the cube of the cylinder tangential velocity and the power coefficient appears to be unaffected by the Reynolds number and on whether the cylinder is spun in an air stream or in still air.

Acknowledgements

This research was supported by the Sea Axe Fund (The Netherlands). The author would like to thank the research sponsor as well as all the staff at Politecnico di Milano wind tunnel for their kind help.

References

Aoki, K., Ito, T., 2001. Flow characteristics around a rotating cylinder. Proc. Sch. Eng. Tokai Univ. 26, 29–34.
Badalamenti, C., 2010. On the Application of Rotating Cylinders to Micro Air Vehicles. Doctoral Thesis. City University, London.
Badr, H.M., Dennis, S.C.R., Young, P.J.S., 1989. Steady and unsteady flow past a rotating circular cylinder at low Reynolds numbers. Comput. Fluids 17, 579–609.
Bergeson, L., Greenwald, C.K., 1985. Sail assist developments 1979-1985. J. Wind Eng. Ind. Aerod. 19, 45–114.
Bordogna, G., Muggiasca, S., Giappino, S., Belloli, M., Keuning, J.A., Huijsmans, R.H.M., van 't Veer, A.P., 2018. Wind-tunnel experiments on a large-scale Flettner rotor. In: Proceedings of the 15th INVENTO Conference, Naples, Italy.
Chew, Y.T., Cheng, M., Luo, S.C., 1995. A numerical study of flow past a rotating circular cylinder using a hybrid vortex scheme. J. Fluid Mech. 229, 35–71.
Clayton, B.R., 1985. BWEA initiative on wind assisted ship propulsion (WASP). J. Wind Eng. Ind. Aerod. 19, 251–276.
Craft, T.J., Iacovides, H., Johnson, N., Launder, B.E., 2012. Back to the future: Flettner-Thom rotors for maritime propulsion?. In: Proceedings of the 7th International Symposium on Turbulence Heat&Mass Transfer, Palermo, Italy.
De Marco, A., Mancini, S., Pensa, C., 2014. Preliminary analysis for marine application of Flettner rotors. In: Proceedings of the 2nd International Symposium on Naval Architecture and Maritime, Istanbul, Turkey.
De Marco, A., Mancini, S., Pensa, C., Calise, G., De Luca, F., 2016. Flettner rotor concept for marine applications: a systematic study. Int. J. Rotating Mach. 2016, 12. Article ID 3458750.
Everts, M., Ebrahim, R., Kruger, J.P., Miles, E., Sharifpur, M., Meyer, J.P., 2014. Turbulent flow across a rotating cylinder with surface roughness. In: Proceedings of the 10th International Conference on Heat Transfer. Fluid Mechanics and Thermodynamics, Orlando, USA.
Flettner, A., 1925. The Flettner Rotorship. Engineering 19, 117–120.
Ingham, D.B., Tang, T., 1990. A numerical investigation into the steady flow past a rotating circular cylinder at low and intermediate Reynolds numbers. J. Comput. Phys. 87, 91–107.
ISO/IEC 98-3, 2008. Guide to the Expression of Uncertainty in Measurement (GUM). International Organization for Standardisation, Geneva, Switzerland.
Karabelas, S.J., 2010. Large eddy simulation of high-Reynolds number flow past a rotating cylinder. Int. J. Heat Fluid Flow 31, 518–527.
Karabelas, S.J., Koumroglou, B.C., Argyropolous, C.D., Markatos, N.C., 2012. High Reynolds number turbulent flow past a rotating cylinder. Appl. Math. Model. 36, 379–398.
Li, D.Q., Leer-Andersen, M., Allenström, B., 2012. Performance and vortex formation of Flettner rotors at high Reynolds numbers. In: Proceedings of the 29th Symposium on Naval Hydrodynamics, Gothenburg, Sweden.
Mittal, S., Kumar, B., 2003. Flow past a rotating cylinder. J. Fluid Mech. 476, 303–334.
Padrino, J.C., Joseph, D.D., 2006. Numerical study of the steady-state uniform flow past a rotating cylinder. J. Fluid Mech. 557, 191–223.
Reid, E.G., 1924. Tests of Rotating Cylinders. Technical Report TN-209. NACA.
Subramanya, K., 2005. 1000 Solved Problems in Fluid Mechanics, second ed. Tata McGraw-Hill, New Delhi.
Swanson, W.M., 1961. The Magnus effect: a summary of investigations to date. J Basic Eng-T Asme. 83, 461–470.
Thom, A., 1934. Effects of Discs on the Air Forces on a Rotating Cylinder. Reports&Memoranda No. 1623. Aeronautical Research Committee.
Tokumaru, P.T., Dimotakis, P.E., 1993. The lift of a cylinder executing rotatory motions in a uniform flow. J. Fluid Mech. 255, 1–10.
Zdravkovich, M.M., 2003. Flow Around Circular Cylinders -, vol. 2. Applications. Oxford University Press, New York.
Zhang, W., Bensow, R., 2011. Numerical simulation of high-Reynolds number flow around Flettner rotors. In: Proceedings of the 14th Numerical Towing Tank Symposium, Southampton, UK.
Zhang, W., Bensow, R., Golubev, M., Chernoray, V., 2013. Flow past a rotating finite length cylinder: numerical and experimental study. In: Proceedings of the 51st AIAA Aerospace Sciences Meeting including the New Horizons Forum and Aerospace Exposition, Grapevine, USA.